Spontaneous aerobic ageing of Fe–N–C materials and consequences on oxygen reduction reaction kinetics

Keyla Teixeira Santos, Kavita Kumar, Laetitia Dubau, Hongxin Ge, Sandrine Berthon-Fabry, Carlos Sant Ana Vasconcellos, Fabio Henrique Lima, Tristan Asset, Plamen Atanassov, Viktoriia A. Saveleva, et al.

Spontaneous Aerobic Ageing of Fe-N-C Materials and Consequences on Oxygen Reduction Reaction Kinetics

*K. Teixeira Santos, [1,‖] K. Kumar, [1,‖] L. Dubau, [1] H. Ge, [2] S. Berthon-Fabry, [2] C.S.A. Vasconcellos, [3] F.H.B. Lima, [3] T. Asset, [4] P. Atanassov, [4] V. A. Saveleva, [5] P. Glatzel, [5] X. Li, [6] F. Jaouen, [7] F. Maillard [1,] **

1. Univ. Grenoble Alpes, Univ. Savoie Mont Blanc, CNRS, Grenoble INP, LEPMI, 38000 Grenoble (France).

2. MINES ParisTech, PSL University, Centre for processes, renewable energy and energy systems (PERSEE), CS 10207, 06904 Sophia Antipolis Cedex, France.

3. Instituto de Química de São Carlos (IQSC), Universidade de São Paulo – Av. Trabalhador São- Carlense, 400 CP 780 – São Carlos – SP.

4. Department of Chemical & Biomolecular Engineering, National Fuel Cell Research Center (NFCRC), University of California Irvine, Irvine, California 92697, United States.

5. ESRF – The European Synchrotron, 71 Avenue des Martyrs, 38000 Grenoble, France

6. Laboratoire de Physique des Solides CNRS, Université Paris Sud, 91405 Orsay, France

7. ICGM, Univ. Montpellier, CNRS, ENSCM, Montpellier, F-34293 Montpellier (France).

‖ These authors contributed equally to this work.

* Corresponding author. Tel.: +33 476 826 592. E-mail address: frederic.maillard@grenoble-inp.fr

Abstract

Tremendous progress in the beginning-of-life oxygen reduction reaction (ORR) activity of iron nitrogen carbon (Fe-N-C) catalysts holds the promise to replace platinum-group metals in proton exchange membrane fuel cells cathode. Improving the understanding of their degradation mechanisms as well as their practical durability are the next two grand challenges. Here, we report on a spontaneous aerobic degradation phenomenon of Fe-N-C materials that takes place upon storage under atmospheric conditions (air, room temperature), and depreciates their electrocatalytic activity towards the ORR. Our study covers a period of 47 months and involves six catalysts, which were synthesized by different laboratories and different methods (sacrificial metal organic framework, silica templating, aerogel-derived, wet impregnation of high surface area carbon black) and which feature distinct morphology, structure and density of active sites. The results from electron and X-ray based techniques indicate that a fraction of the single Fe atoms spontaneously transforms into Fe or Fe-oxide aggregates over time, in line with the decrease in the active site density measured by *in situ* nitrite stripping. Along with these structural changes, a strong decrease in ORR turnover frequency was also observed. These adverse effects can be mitigated using storage under dry and oxygen-free atmosphere.

Keywords: Oxygen reduction reaction; Fe-N-C electrocatalysts; Carbon corrosion; Fe demetalation; Stability; Mitigation strategy.

1. Introduction

Human activities release massive amounts of greenhouse gas in the atmosphere. Proton-exchange membrane fuel cell (PEMFC) running on air and renewably-produced hydrogen could efficiently mitigate global warming; however, this technology uses scarce and expensive platinum-group metals (PGMs) to electrocatalyze the cathodic oxygen reduction reaction (ORR). To replace PGMs at the PEMFC cathode, research focuses on transition metal atoms embedded into nitrogen-doped carbon matrix (Metal-N-C) catalysts, and Fe-N-C has been identified as the most active Metal-N-C catalyst for the ORR [1-3]. Fe-N-C catalysts can be prepared by: i) pyrolysis of Fe macrocycles (phthalocyanines, porphyrins, tetraazaannulene, *etc*), carbon (C) and nitrogen (N) precursors [4, 5] ii) pyrolysis of Fe-N-C precursors prepared from Fe salts, C and N organic precursors and securing mesoporosity via a hard templating with silica, [6] iii) pyrolysis of Fe-N-C precursors prepared from iron salt and metal-organic frameworks (MOF) (soft templating), [7-9] iv) pyrolysis of Fe-N-C precursors prepared from Fe salts and polymers [10] or v) vapor deposition of Fe onto a preexisting N-C support [11-13]. Each of these synthesis methods can be fine-tuned to achieve single Fe atoms coordinated to four nitrogen atoms (FeN_4), identified as the most active sites toward the ORR. A rapid drop in ORR performance is frequently reported within the first hours of operation in thin-film rotating disk electrode (RDE, liquid electrolyte) or in PEMFC systems (solid electrolyte) [14, 15], followed by a slower but continuous performance decay [16, 17]. Hence, the identification of degradation mechanisms of Metal-N-C catalysts and the development of mitigation strategies has recently become the focus of several research groups worldwide [14, 18-23]. For the most mature Fe-N-C catalysts, it has long been thought that demetallation of FeN_x sites was the primary degradation mechanism in acidic media [18, 19, 21]. However, experimental and theoretical studies have reported that FeN_x

sites are relatively stable in the potential range of 0 – 1 V *vs*. the reversible hydrogen electrode (RHE) in O_2-free acidic electrolyte [19, 24-26]. Recent findings from Kumar *et al*. in RDE [14] and Osmieri *et al*. in PEMFC device [15] have established that the combination of high electrochemical potential and presence of O_2 is a major stressor of Fe-N-C catalysts. Indeed, free Fe cations (and even FeN_x sites) react with hydrogen peroxide (H_2O_2), a well-known ORR intermediate, yielding reactive oxygen species (ROS) such as superoxide ($^{\bullet}O_2^-$), hydroxyl ($^{\bullet}OH$) and hydroperoxyl ($^{\bullet}OOH$) radicals. These radicals readily corrode the carbon matrix, leading *in fine* to the destruction of FeN_x sites, and their release as free Fe cations with the exhaust water or their reprecipitation into ORR-inactive Fe nano-oxides (FeO_x). Carbon oxidation reaction (COR) also partially accounts for the drop in ORR performance of Fe-N-C catalysts. In acidic electrolyte, bulk COR takes place at electrode potentials higher than 1.0 V *vs*. RHE and its rate is strongly accelerated by temperature [20, 27, 28]. Surface COR is, by definition, restricted to the formation of oxygen-containing surface groups, without irreversible release of C atoms as carbon monoxide (CO) or carbon dioxide (CO_2) gas [20]. Despite the mild surface oxidation, the oxygen-surface groups modify the π-electron delocalization around the FeN_x sites, leading to a drop of their turnover frequency (TOF) [2, 20]. Similarly, the protonation of highly basic N groups (typically, occurring during their immersion in acidic electrolyte or solid proton conductors) alters the electronic structure of FeN_x sites and depreciates their TOF. The latter degradation mechanism is more marked for catalysts that are (re)pyrolised under ammonia (NH_3) in the last stage of their synthesis [22, 29]. In parallel to the fast degradation of the ORR performance observed at the beginning of life, Boldrin *et al*. [30] recently reported a drop in ORR activity of Fe-N-C catalysts after one year of atmospheric storage. The authors argued that the adsorption of water or oxygen species onto the carbon surface leads to the formation of

oxygen-containing surface groups (such as epoxides, then aldehydes over time), which modify the electronic environment of the FeN_x sites in a way similar to surface COR [20]. Partial recovery of the ORR performance loss observed after one-year storage by heat treatment (600°C, argon (Ar), 1h) or by reductive treatment (-0.3 V *vs*. RHE, 30 s) supported the author's claim.

Similarly to what was shown by Boldrin *et al.* [30], in this study, we report a drop of the ORR activity over time for six Fe-N-C catalysts prepared using different synthetic approaches (hard templating with silica, carbonization of metal organic framework, aerogel chemistry, wet impregnation of high surface area carbon black), and thus featuring distinct textural, structural and chemical properties. However, in contrast to Boldrin *et al.* [30], we show that the loss of ORR activity could not be recovered by electrochemical reductive treatment, but only by the 600° C treatment in Ar, likely due to the longer aging time investigated here, up to 4 years.

2. Experimental

2.1. Electrocatalysts

The six Fe-N-C catalysts investigated in this study were synthesized by different academic laboratories and analyzed in their pristine state and after different ambient storage durations. The ZIF-8-derived Fe-N-C catalysts from CNRS – University of Montpellier were produced either by ramp pyrolysis from room temperature to 1050°C at 5°C min^{-1}, then 1 h dwell time at 1050°C under Ar (**CNRS-RP**) or flash pyrolysis by inserting directly the catalyst precursor in the oven pre-equilibrated at 1050°C, 1 h dwell time at 1050°C under Ar (**CNRS-FP**). They were formerly labeled as $Fe_{0.5}$ RP and $Fe_{0.5}$ FP in Ref. [21]. Detailed physicochemical characterization can be found in Ref. [7]. Two other Fe-N-C catalysts, derived from nicarbazin, were prepared by University of California Irvine using hard silica template, and single (**UCI-1**) or double (**UCI-2**)

pyrolysis steps. The first pyrolysis was performed at T = 975°C (ramp pyrolysis, 31.25 °C min^{-1} from 525°C to 900°C, 9.4 °C min^{-1} from 900°C to 975°C, hold for 45 min at 975°C) in N_2:H_2 gas mix 93:7, and the second pyrolysis at T = 950°C (flash, 30 min) in N_2:NH_3 gas mix 90:10. They were previously referred to as Fe-HT1 and Fe-HT2, respectively and have been thoroughly characterized in Ref. [22]. A modified pre-polycondensation method was used to prepare a Fe-N-C aerogel catalyst (**ARMINES**) at MINES Paristech using a one-pot synthesis protocol first introduced in Ref. [31]. The Fe, N and C precursors were all introduced into the sol simultaneously. The resulting gels were dried and pyrolised at 800 °C in N_2 for 1 h, followed by a second pyrolysis at 950 ◦C under flowing N_2:NH_3 gas mixture 90:10 for 45 min. To remove Fe nanoparticles, acid washing was performed in 0.5 M H_2SO_4 at 80°C for 7 h between the two pyrolysis steps. Finally, a Fe-N-C material was synthesized by Universidade de São Paulo (**IQSC**) using the strategy previously introduced by Zhang *et al*. [5]. In brief, 1,10-phenanthroline (Sigma-Aldrich) was dissolved in ethanol, followed by the addition of $Fe(NO_3)_3.9H_2O$ (Merck, 99.95%), and the system was maintained under reflux. Black Pearls®2000 (Cabot Corp.) carbon powder was added to the as formed tris(1,10-phenanthroline)iron(II) complex, and the system was opened for solvent evaporation. The resulting powder was heat treated in a tubular oven under Ar atmosphere, at 1050 °C, for 1 h. All electrocatalysts were stored in closed flasks (Qorpak™ Clear Borosilicate Sample Vials with Caps type) over a period of 47 months in total. For the sake of understanding and mitigating ORR activity losses, a given amount of the ARMINES catalyst was also stored in a desiccator for 24 months and another one in an Ar box for the same amount of time. A flask containing CNRS-FP catalyst was also kept in an Ar box for 24 months. The same ageing was conducted on a Co-N-C material synthesized using the same synthesis protocol than CNRS-RP (Co-CNRS-

RP), and first introduced in Ref. [21] and on a benchmark 20 wt. % Pt/Vulcan XC72 catalyst (TEC10V20E from Tanaka Kikinzoku Kogyo, TKK).

2.2. Transmission electron microscopy (TEM) and energy dispersive X-ray spectroscopy (X-EDS)

The Fe-N-C materials were observed by TEM and analyzed via X-EDS in their pristine form and after storage in closed flasks for different amount of time. We used a TEM JEOL 2010 with a resolution of 0.19 nm and operated it at 200 kV. X-EDS analyses were performed in five different Fe-based particle-free regions of the TEM grid. Quantification of the Fe content was performed using the Fe *K* line and the *K*-factors provided by the software.

2.3. High-angle annular dark-field scanning transmission electron microscopy imaging (HAADF-STEM)

HAADF-STEM images were obtained using a Nion UltraSTEM 200, equipped with C3/C5 aberration corrector. The instrument was operated at 60 kV to mitigate the beam damage. The convergence semi-angle was 33 mrad, while the inner and outer collection semi-angle of HAADF detector were 70 and 210 mrad, respectively.

2.4. Scanning transmission electron microscopy (STEM)

The STEM/X-EDS elemental maps were acquired using a JEOL 2100F microscope operated at 200 kV equipped with a retractable large angle Centurio Silicon Drift detector. We used the Fe *K*, C *K* and O *K* lines and the *K*-factors provided by the JEOL software.

2.5. X-ray absorption spectroscopy (XAS) and X-ray emission (XES) spectroscopy

Fe *K*β high energy-resolution fluorescence-detected X-ray absorption near edge structure (HERFD-XANES) and *K*β XES spectra were recorded at beamline ID26 at the European Synchrotron Radiation Facility (ESRF), Grenoble, France. Si (111) double-crystal monochromator was used for the measurements. The maximum of Fe *K*β fluorescence line (7.058 keV) was selected with an emission spectrometer in Rowland geometry with five Ge (620) analyser crystals (Bragg angle, 79°). The incident beam absolute energy calibration was performed using a reference metallic Fe foil by setting the first inflection point of the Fe *K* edge at 7112 eV. The incident energy was varied from 7100 to 7200 eV over Fe *K* edge. HERFD-XANES spectra were recorded in continuous mode during 20 sec with an energy step of 0.1 eV, where at least 15 spectra collected at different spots on the sample were averaged. The XES spectra were collected with a step size of 0.1 eV and an incident energy of 7800 eV. The analysed catalyst powders were sealed in the Kapton tubes (external diameter – 3.0 mm, thickness – 0.03 mm, GoodFellow), the spectroscopic measurements were performed at room temperature and under air. HERFD-XANES and XES spectra were normalized in area using the ranges 7100 – 7200 eV and 7030 – 7070 eV, respectively.

2.6. X-ray photoelectron spectroscopy (XPS)

The X-ray photoelectron spectra were obtained using a Kratos Axis DLD Ultra XPS, with an Al K_α monochromatic source operating at 150 W. The operating pressure was 2×10^{-9} Torr. The high-resolution spectra in the C1s and N1s region were obtained with a pass energy of 20 eV, 3 min of acquisition time for C1s and 40 min of acquisition time for N1s. The data was acquired on three different regions. CasaXPS was used for the data analysis. A linear background subtraction was used and a 70 % Gaussian/30 % Lorentzian shape was used for the curve fitting. N1s was fitted with an established set of components based on previous study [32].

Deconvolution of the C1s narrow scan spectrum into different functional groups considered C–C (sp2 and sp3-hybridized carbon atoms, 284.7 and 287.9 eV, respectively), C–N (carbon atoms near N-containing moieties at *ca*. 286 eV), and oxygen-containing surface groups (hydroxyl, epoxy, ethers, carbonyl and/or quinone-like, carboxylic acid, lactone, anhydride ranging from *ca.* 287 to 293 eV).

2.7. Electrochemical measurements

Catalyst's suspensions were prepared by mixing of 10 mg of each material, 50 μL of a Nafion solution (5 *wt.*% in a mixture of lower aliphatic alcohols and water), 854 μL of 2-propanol and 372 μL of ultrapure water (Millipore, 18.2MΩ cm, total organic compounds < 3 ppb). An aliquot was then drop-casted onto a glassy carbon disk (5 mm diameter, Sigradur G from Hochtemperatur- Werkstoffe GmbH) embedded in polychlorotrifluoroethylene cylinder and used as working electrode. The catalyst's loadings were 800 and 300 μg_{powder} cm^{-2} for electrochemical characterizations and electrochemical quantification of the active sites, respectively. For IQSC, a catalyst's loading of 600 μg_{powder} cm^{-2} was used for the electrochemical characterizations.

To avoid organic contamination, all glassware used in this study was previously cleaned using Caro's acid (50 % v/v of H_2SO_4/H_2O_2) and then boiled in ultrapure water (Millipore, 18.2 MΩ cm, 1−3 ppm total organic compounds) before being used. We used a three-electrode cell composed of: (i) a glassy carbon plate as counter-electrode; (ii) a commercial reversible hydrogen electrode (RHE, Hydroflex, Gasktel GmbH) and (iii) a thin-film rotating disk electrode as working electrode. The electrodes were electrically connected using a bi-potentiostat equipped with a potentiostat with an analog linear scan generator (Autolab PGSTAT302N) and NOVA 2.0

software was used to record the electrochemical measurements. All electrode potentials are referred to the reversible hydrogen electrode (RHE).

Prior to the RDE measurements, the electrolyte was deaerated with Ar (> 99.999 %, Messer), and 50 cyclic voltammograms (CVs) between 0.0 and 1.0 V were performed at 100 mV s^{-1} in Ar-purged 0.1 mol L^{-1} H_2SO_4 electrolyte ('break-in cycles') followed by 3 CVs at 10 mV s^{-1} and 1 CV at 2 mV s^{-1} ('characterization cycles'). The 2 mV s^{-1} cycle served to correct the ORR polarization curves for pseudocapacitive currents. The ORR polarization curves were performed between 0.0 and 1.0 V *vs*. RHE, at 1600 rpm, T = 25 °C in O_2-saturated 0.1 M H_2SO_4 electrolyte. For the IQSC catalyst, the electrochemical measurements were performed in 0.5 M H_2SO_4 and v = 50 mV s^{-1} for the CVs and v = 5 mV s^{-1} for ORR polarization curves.

The quantification of the active sites was performed using the *in situ* electrochemical method, firstly reported by Malko *et al*. [33] The thin-film RDE was firstly cleaned by performing different CVs in Ar- and O_2-saturated acetate buffer solution (pH 5.2). The catalyst was then poisoned using a nitrite solution (0.125 M of $NaNO_2$). After one CV between 1.0 and 0.3 V *vs.* RHE, nitrite stripping was recorded. The excess coulometric charge measured before and after nitrite stripping was used to calculate the number of catalytic sites located at the surface of a catalyst (site density, SD, sites g^{-1}_{powder}) assuming 5 electrons exchanged per NO, and one NO adsorbed per active site:

$$\mathrm{SD} = \frac{Q_{\mathrm{strip}} \times N_{\mathrm{A}}}{n_{\mathrm{strip}} \times F} \qquad \textbf{(Equation 1)}$$

Where Q_{strip} (C g^{-1}_{powder}) and n_{strip} refer to the excess coulometric charge and the number of electrons, respectively, N_A (mol^{-1}) and F (C mol^{-1}) represent the Avogadro number and Faraday

constant, respectively. The Fe-N-C loading for all *in situ* nitrite stripping experiments was 0.3 mg cm^{-2}.

From SD and MA (the mass activity (A g^{-1}_{powder}) measured at E = 0.8 V *vs*. RHE in 0.1 M H_2SO_4 for CNRS, UCI, ARMINES, or 0.5 M H_2SO_4 for IQSC), the turnover frequency (TOF, s^{-1}) for the ORR could be determined:

$$\text{TOF}\ (s^{-1}) = \frac{MA_{0.80} \times N_A}{SD \times F} \qquad \textbf{(Equation 2)}$$

3. Results

3.1. Physicochemical properties of the fresh catalysts

Insights into the carbon morphology and the average Fe content of the six Fe-N-C catalysts were gained using TEM images and point X-EDS analyses. As most of the catalysts (except the IQSC and the ARMINES catalysts) used in this study have been extensively characterized in our former works [14, 21, 22], we here briefly summarize the main findings. As shown in **Figure 1 (a-b)**, the CNRS-RP and CNRS-FP catalysts are composed of stacked carbon sheet-like layers. The Fe content was 0.79 ± 0.34 and 0.99 ± 0.55 at. % for CNRS-RP and CNRS-FP, respectively (**Figure 1g**) and former extended X-ray absorption fine structure (EXAFS) and ^{57}Fe Mössbauer spectroscopy characterizations established that CNRS catalysts contain only or mostly FeN_x moieties [14, 21]. The same holds true for the UCI catalysts, composed of atomically dispersed single Fe atoms embedded into stacked graphitic sheets (**Figure 1c** and **Figure 1d**) [22]. X-EDS analyses indicated a lower Fe content for this group of catalysts: 0.08 at. % and 0.14 at. % for the UCI-1 and UCI-2, respectively (**Figure 1g**). For the IQSC catalyst (**Figure 1e**), the X-EDS analyses indicated a lower Fe content, 0.09 at. %, and the TEM image shows the absence of any

Fe particle or cluster in agreement with the aberration-corrected HAADF-STEM and XAS analyses of Ref. [5]. Finally, TEM images showed that the aerogel Fe-N-C catalyst synthesized by ARMINES is composed of spherical nanoparticles connected to each other, with inter-particle pore size ranging from few nm to > 100 nm. In this synthesis, inspired from the work described in Ref. [31], an acid washing step is performed between the two pyrolysis (first one under N_2 and second one under N_2:NH_3 mix) to remove metallic Fe, Fe oxide and Fe carbide nanoparticles, and this was verified using EXAFS and ^{57}Fe Mössbauer spectroscopy [31, 34]. Summing up, all synthesized materials thus feature atomic dispersion of Fe atoms but had distinct textural, structural and chemical properties.

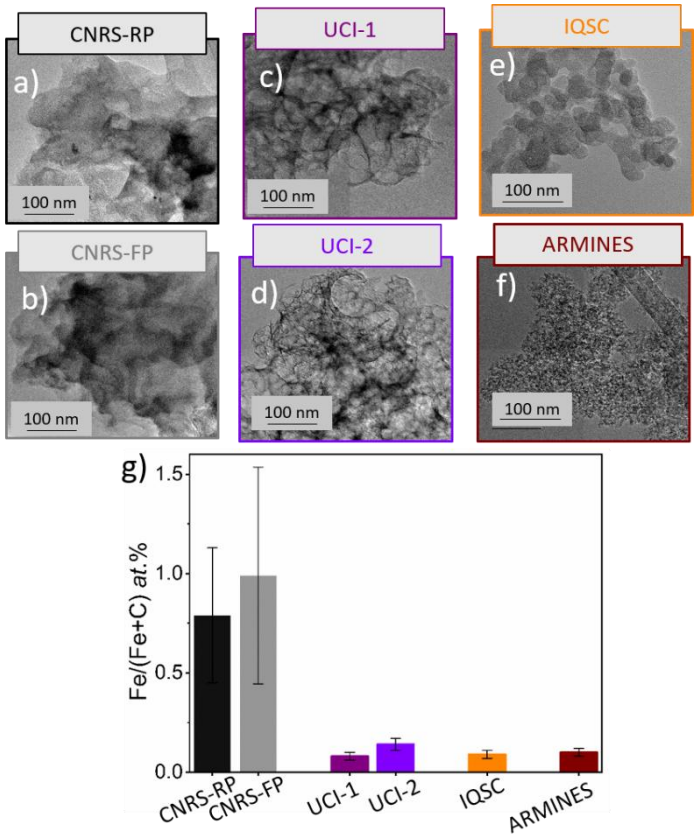

Figure 1. a-f) Representative TEM images and g) Fe content measured by local X-EDS analyses in at least five different particle-free zones for the six Fe-N-C catalysts used in this study.

3.2. Electrochemical properties of the fresh catalysts

The ORR mass activity (MA) of five out of the six Fe-N-C catalysts investigated in this study was assessed in 0.1 M H_2SO_4 with conventional RDE set-up at LEPMI while that of the IQSC catalyst was determined in 0.5 M H_2SO_4 at IQSC. As-measured ORR curves and CVs can be found in **Figure S1**, from which the MA values were derived after corrections for iR (Ohmic) drop, pseudocapacitive current, and O_2 diffusion limitation. Because MA depends on the number of catalytic sites located at the surface of a catalyst (SD) and on the turnover frequency at a given *E,* the SD values were determined using the *in situ* nitrite stripping method that was first introduced by Malko *et al.* [33]. The TOF was then calculated by combining MA values measured in 0.1 (or 0.5) M H_2SO_4 and SD values (**Equation 2**). It is noteworthy that, despite their similar Fe content (**Figure 1g**), the two CNRS catalysts perform differently towards the ORR, with CNRS-RP being much more active than CNRS-FP (**Figure 2a**). As revealed by **Figure 2b** and **Figure 2c**, better ORR performance of CNRS-RP compared to CNRS-FP results from its 5-fold higher TOF, despite a *ca*. 2-fold lower SD. For the UCI catalysts group, the double-pyrolysed UCI-2 catalyst was more active than the UCI-1 catalyst, in line with the conclusion of Koslowski *et al.* that a second pyrolysis under ammonia introduces more N moieties on the carbon surface and reveals FeN_x active sites initially hidden in the bulk of the carbon matrix due to its etching (HCN and CH_4 production) [35]. The higher SD and TOF values for the UCI-2 catalyst compared to the UCI-1 catalyst support this conclusion (**Figure 2b** and **Figure 2c**). A high SD but a low TOF value were measured for the ARMINES catalyst. High SD is in line with its highly porous texture (see BET surface area (S_{BET}) in **Table S1** and **Figure S2**) but its lower TOF value compared to those of CNRS, UCI and IQSC catalysts was surprising. Indeed, the ARMINES catalyst experienced a dual pyrolysis (first pyrolysis at 800 ◦C in N_2 for 1

h, second pyrolysis at 950 ◦C under flowing N_2:NH_3 gas mixture 90:10 for 45 min), which should have led to high TOF value as discussed in the above. The poor degree of graphitization of this catalyst in comparison to others (see *L*a, *L*c and interlayer spacing values in **Table S1**) may account for such low TOF. Indeed, in turbostratic carbons, high electrical conductivity is usually found parallel to the quasi-graphitic layers due to the delocalized π-electrons, whereas low conductivity prevails perpendicular to the quasi-graphitic layers. Last, the IQSC catalyst featured similar TOF as the UCI-1 and CNRS-RP catalysts, however the conventional ion complexation/adsorption/pyrolysis approach used for its synthesis led to a lower SD value.

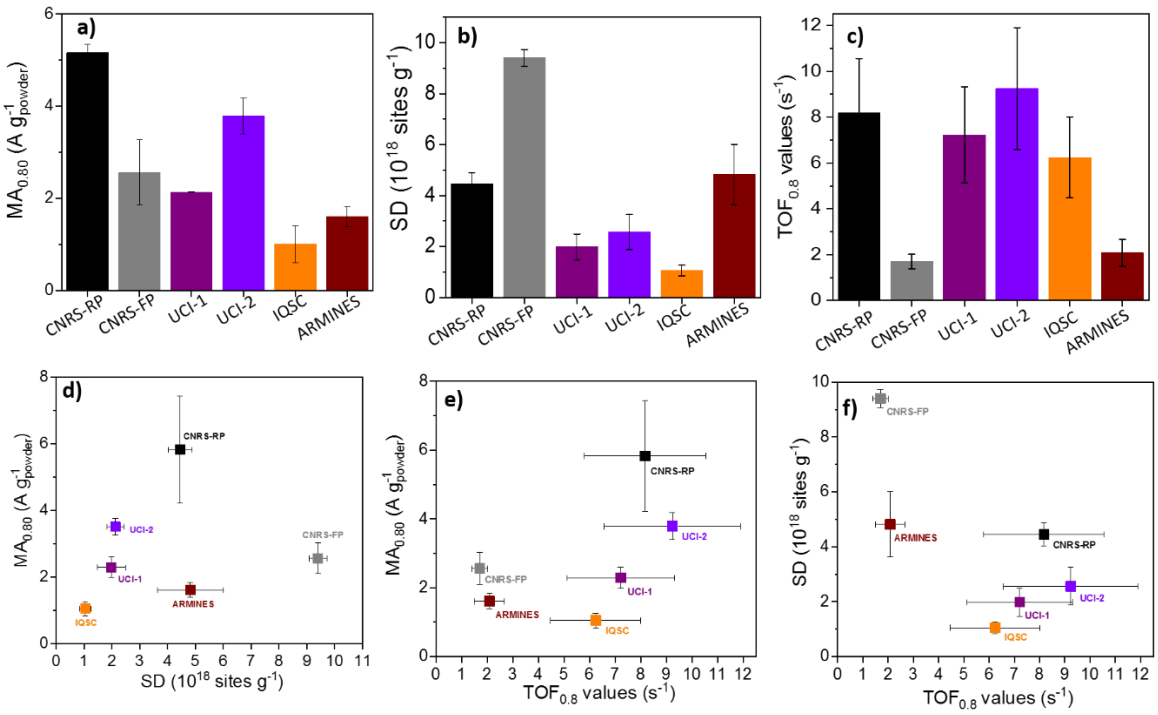

Figure 2. Electrochemical characterizations of the six Fe-N-C catalysts used in this study: (a) ORR mass activities measured at E = 0.8 V *vs.* RHE ($MA_{0.80}$) in O_2-saturated 0.1 M H_2SO_4 at v = 2 mV s^{-1} and ω = 1600 rpm. The catalyst loading was 0.8 mg cm^{-2}_{geo} for all catalysts except for the IQSC catalyst (0.6 mg cm^{-2}) for which the electrochemical measurements were performed

in 0.5 M H_2SO_4 at v = 5 mV s^{-1} and ω = 1600 rpm, b) active site density (SD) values measured in acetate buffer electrolyte (pH = 5.2) using the *in situ* nitrite chemisorption method, c) TOF values (calculated from the $MA_{0.80}$ and SD values). For $MA_{0.80}$ and SD, the error bars are the standard deviation obtained from at least two different measurements and for TOF, the error bars represent the relative error of $MA_{0.80}$ and SD values. Correlation between d) $MA_{0.80}$ and SD, e) $MA_{0.80}$ and TOF, f) SD and TOF.

The correlations between MA, SD and TOF values represented in **Figure 2d, Figure 2e** and **Figure 2f** provide insights on how each group of materials catalyzes the ORR, and how their intrinsic activity could be enhanced. Low SD values catalysts (IQSC, UCI) call for increased Fe content or electrochemically accessible surface area. In turn, catalysts with low TOF values (ARMINES, CNRS-FP) call for modifications of the synthesis protocol towards more favorable chemical environment for the FeN_x sites.

3.2. Spontaneous decrease of the ORR mass activity upon storage in closed flasks in atmospheric conditions

Figure 3 illustrates how the ORR activity changes upon storage under atmospheric conditions in closed flasks over a period of 47 months (note that the flasks were not pumped before storage). A marked decrease of MA was observed for all catalysts independently from their synthesis protocols. Also obvious from **Figure 3a** is the fact that the rate at which the MA decreased is catalyst-dependent, and seems related to the initial MA value. Indeed, **Figure 3b** displays a correlation between the MA remaining after Δt months (with Δt = 48 months for IQSC and 47 months for CNRS-RP, CNRS-FP, UCI-1 and UCI-2 catalysts) and the initial MA, except for

CNRS-FP. The latter is the only material that was prepared with a flash pyrolysis method, possibly explaining why it is an outlier.

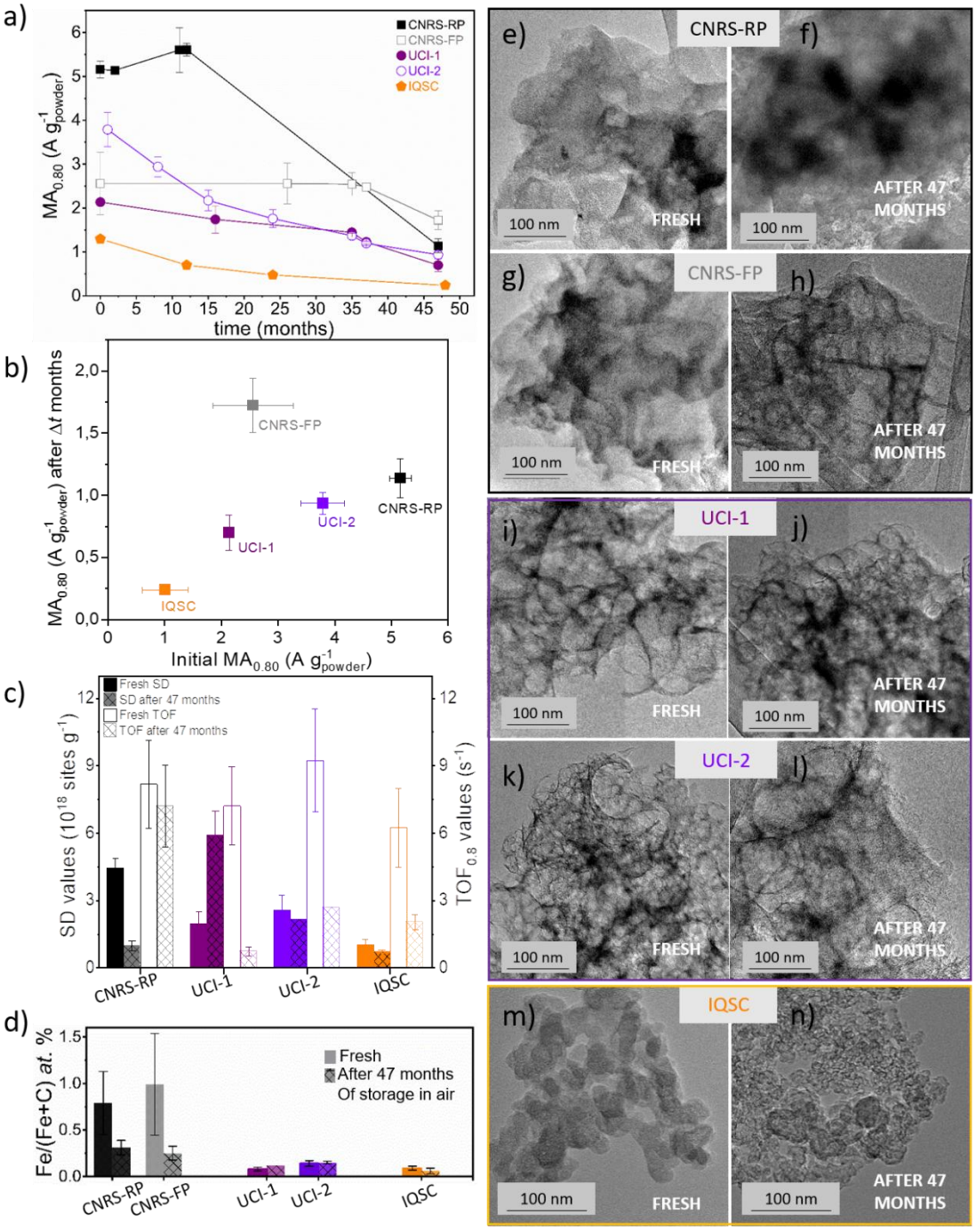

Figure 3. a) Time-dependency of the ORR mass activity for five Fe-N-C catalysts; b) Correlation between the MA remaining after Δt months (with Δt = 48 months for IQSC and 47 months for the other four catalysts) and the initial MA. The mass activities were measured at E = 0.80 V *vs.* RHE in O_2-saturated 0.1 M H_2SO_4 at v = 2 mV s^{-1} and ω = 1600 rpm. The catalyst loading was 0.8 mg cm^{-2}_{geo} for all materials except for the IQSC material, for which 0.6 mg cm^{-2} was used and the electrochemical measurements were performed in 0.5 M H_2SO_4 at v = 5 mV s^{-1} and ω = 1600 rpm, c) SD and TOF values for the fresh and the 47-month aged CNRS-RP, UCI-1, UCI-2, and IQSC catalysts. For MA and SD, the error bars are the standard deviation obtained from at least two different measurements and for TOF, the error bars represent the relative error of MA and SD values. d) Fe content measured by X-EDS and representative TEM images of the fresh and the 47 month-aged catalysts. The Fe content was measured by X-EDS in at least five different aggregate/nanoparticle-free regions of the fresh/aged catalysts.

The variations of SD and TOF values over time for the CNRS-RP, UCI-1, UCI-2, and IQSC catalysts are displayed in **Figure 3c** and brutto *in situ* nitrite stripping data can be found in **Figure S3**. The SD values dropped for the CNRS-RP (-78 %), the IQSC (-30 %) and the UCI-2 (-15 %) catalysts. The trend was opposite on the UCI-1 catalyst (+200 % in SD), indicating that a higher number of Fe atoms is exposed at the surface, most likely as a result of the corrosion of the N-C matrix (which will be discussed later in this manuscript). However, as nitrite stripping not only senses surface Fe-N_x sites but also Fe-oxides (Fe-O_x), [14] the coordination of the additional Fe atoms (Fe-N_x or Fe-O_x sites) measured by nitrite stripping for the aged UCI-1 relative to the pristine UCI-1 remains ambiguous. The SD of Fe-N_x sites may even have decreased from the pristine UCI-1 to the aged UCI-1, and be overcompensated by a strong increase in surface FeO_x sites. Regardless of the synthesis protocol and of the pyrolysis

atmosphere, the use of MOF as precursors and the resulting high microporosity of the Fe-N-C seem to limit the drop in the TOF value, as the intrinsic activity of the FeN_x moieties is mostly maintained on CNRS-RP (-12 %), whereas the other catalysts exhibit a relative decrease in TOF ranging from -68 % and -71 % (IQSC and UCI-2, respectively) to -90 % (UCI-1). The strongest decrease in TOF observed for UCI-1 further supports that the increase in SD observed during aging of UCI-1 is related to carbon corrosion, forming FeO_x atoms/clusters on the surface from initially bulk FeN_x sites. As FeO_x has very low ORR activity (low TOF) but is sensed by nitrite stripping, this would contribute to further lowering the average TOF measured for the aged UCI-1 material (as the TOF is obtained by dividing the overall mass activity by the overall SD).

3.3. Changes in structure and chemistry after 47 months of storage in closed flasks

TEM images and point X-EDS analyses of the fresh and aged catalyst powders confirmed the trends derived from the *in situ* nitrite stripping method. Indeed, **Figure 3 e-n** indicate little to no change of the carbon matrix morphology for the catalysts pyrolysed under Ar atmosphere (CNRS-RP, CNRS-FP and IQSC). However, X-EDS analyses performed on five different particle-free zones indicated a decrease of 61 and 33 % in the Fe content after 47 months of storage for CNRS-RP and after 48 months of storage for IQSC electrocatalysts, respectively (**Figure 3d**). Despite the incertitude related to each characterization technique, these values are in excellent agreement with the 78 % and 30 % decrease of the SD value reported for these two catalysts in **Figure 3c**. Discussing the different Fe content losses between CNRS-RP and IQSC catalysts, we underline that the IQSC synthesis method uses a pre-existing conductive carbon powder, while CNRS-RP uses as a carbon source the carbon atoms present in the methylimidazole ligand of the MOF ZIF-8 and also the carbon atoms present in phenanthroline (no existing conductive carbon phase in CNRS-RP synthesis before the pyrolysis step). The two

methods result in nearly equivalent BET surface area but higher Fe content and SD value for CNRS-RP in comparison to IQSC catalyst (0.79±0.34 *vs*. 0.09±0.02 at. % and 4.45±0.45 10^{18} *vs*. 1.05±0.21 10^{18} sites $g^{-1,}$ see **Table S1**). The higher Fe at. % is believed to facilitate the aggregation of single Fe atoms over time, and to account for the most pronounced drop in local Fe content measured by X-EDS for CNRS-RP *vs*. IQSC. For the UCI-1 catalyst, the Fe content in particle-free zones slightly increased after 47 months (0.08 ± 0.02 at. % and 0.12 ± 0.00 at. % for the pristine and the 47-month aged UCI-1 catalyst), in qualitative agreement with the increased SD. In contrast, no change of the local Fe content in particle-free zones was observed for the UCI-2 electrocatalyst, in line with its slight decrease in SD after 47 months storage (**Figure 3c**). As the overall Fe content should be identical in a fresh and an aged catalyst for ambient storage (no possible gain or loss in Fe) and as analyses were performed in particle-free areas, slightly increasing Fe content monitored by local X-EDS analyses in particle-free areas confirms that the carbon matrix was slightly corroded *i.e*. that Fe atoms initially positioned in sublayer(s) of the carbon matrix became exposed at the surface during ageing. Nevertheless, COR was probably restricted to the outermost surface layers as Raman spectra (not shown) showed no change in the bulk carbon structure (Raman spectroscopy is a bulk technique).

To gain atomic-scale insights, we used Cs-corrected atom-resolved high-angle annular dark-field scanning transmission electron microscopy (HAADF-STEM). The HAADF-STEM images of the pristine, 2-year and 4-year aged UCI-2 catalysts displayed in **Figure 4a** confirmed atomic dispersion of Fe atoms for the fresh UCI-2 catalyst but also revealed that small Fe aggregates with sizes comprised between 3 and 5 nm are present after 2 years of ageing under atmospheric conditions (**Figure 4b**). The fraction of aggregated nanoparticles increased for the 4 year-aged catalyst (**Figure 4c** and **Figure 4d**). To give a statistical value to our measurements, HAADF-

STEM images were also taken in other areas of the fresh and aged UCI-2 catalyst: they show the same phenomena, in the same proportions. The HAADF-STEM images therefore indicate that aggregation occurred only to a minor extent and could not account for the 15 % decrease in SD observed for this catalyst over a period of time of 47 months.

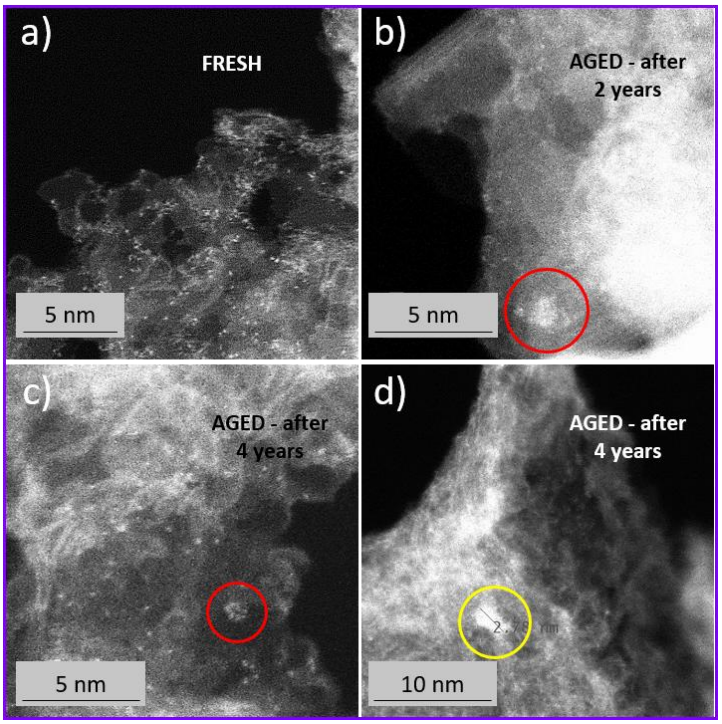

Figure 4. HAADF-STEM images of the UCI-2 catalyst a) before or after b) 2 years or c-d) 4 years of storage in closed flasks under atmospheric conditions. Fe aggregates (group of Fe atoms located close to each other, but not necessarily in a crystalline structure) are highlighted by the red and yellow cycles, respectively.

STEM images and elemental mapping were also recorded for some catalysts in their pristine or aged state. For catalysts pyrolised by ramp mode under inert gas or inert gas / H_2 mix (CNRS-RP, UCI-1), STEM images confirmed the presence of Fe-based aggregates after 47 months of storage under air (**Figure 5a, c** and **Figure 5d, f**). These aggregates might contain minor traces

of oxygen, as suggested by elemental maps displayed in **Figure 5b** and **Figure 5e**, with slightly higher oxygen signal at the agglomerate's location.

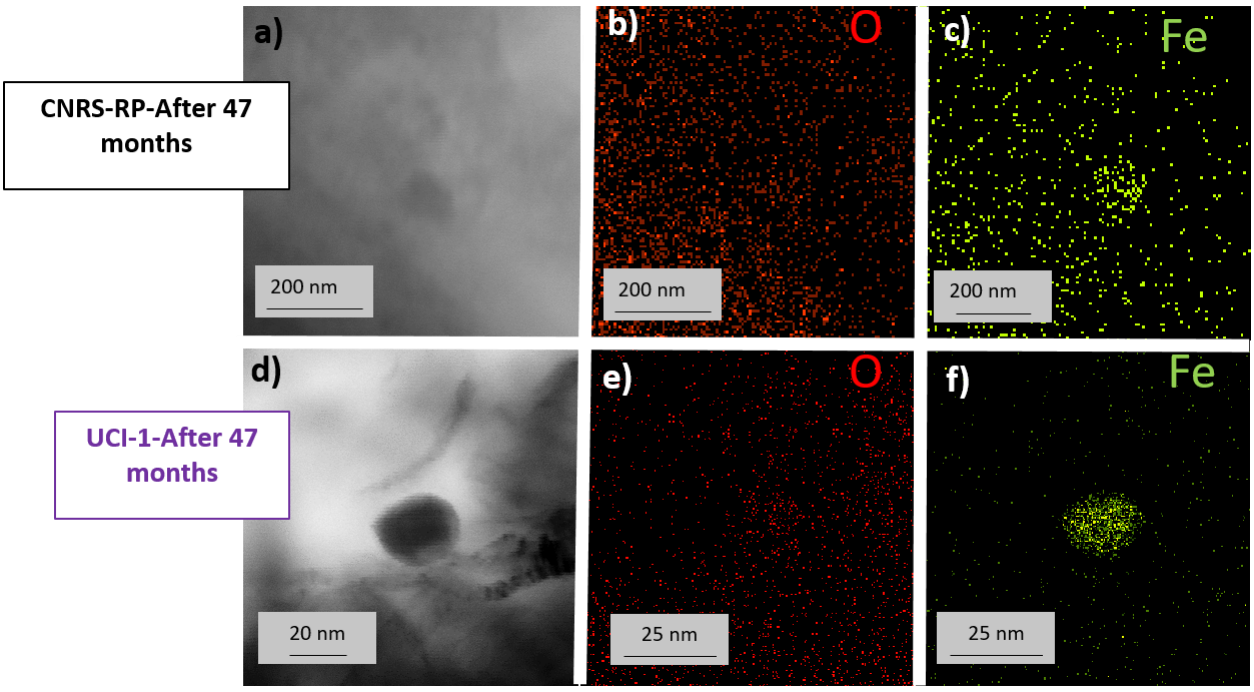

Figure 5. Scanning transmission electron microscopy images and associated X-EDS elemental maps for the (a-c) CNRS-RP, (d-f) UCI-1 catalysts after Δt = 47 months. The elemental maps were built using the Fe *K*, C *K* and O *K* lines. The red and green colors correspond to the oxygen and iron atoms, respectively.

HERFD-XANES and Kβ XES spectra measured on the fresh and the aged CNRS-RP catalyst are displayed in **Figure 6**. In comparison to regular fluorescence-XAS, HERFD-XANES data provides sharper energy resolution that improves the accuracy of the XANES analysis, moreover, the XAS spectra obtained by measuring fluorescence line (*K*β in this case) are spin or ligand sensitive [36].

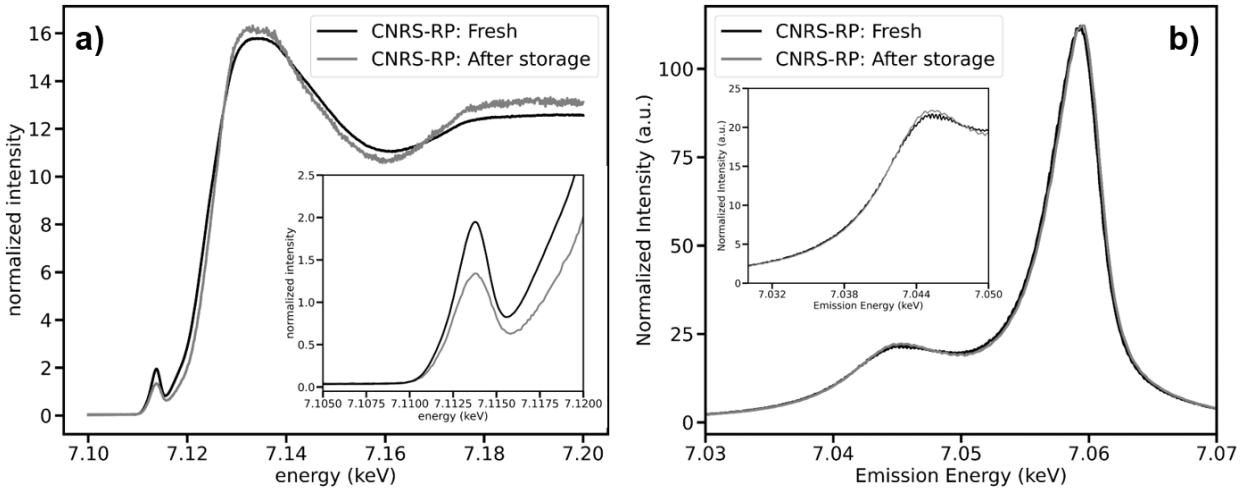

Figure 6. Kβ HERFD-XANES (a) and XES (b) spectra recorded on a fresh and after storage CNRS-RP sample. The insets show zoomed area of pre-edge region (a) and Kβ' shoulder.

The changes in the spectra after storage of the CNRS-RP catalyst provide evidence for an increase of the average oxidation state of Fe via increase of the Fe *K* edge white line intensity (**Figure 6a**) and slight growth in the average spin state of Fe atoms based on the shift of *K*β mainline towards higher energies (**Figure 6b**) coupled with increase of *K*β' shoulder intensity (inset of **Figure 6b**). Changes in Fe electronic structure are typically accompanied by the reorganization of the local coordination sphere around Fe. The latter can be tracked by the analysis of the Fe pre-edge features resulting from 1s → 3d transitions (inset of **Figure 6a)**, where the shrink of the pre-edge intensity observed for the aged CNRS-RP catalyst can be attributed to a decrease in the ratio between 4-fold and 5-/6-fold coordinated sites [37]. This supports that an increased fraction of Fe cations was exposed to the surface or became axially coordinated. A significant part of the signal of the Mössbauer spectrum of the fresh CNRS-RP catalyst is related to the quadrupole doublet D2, assigned to a Fe(II)-N_4 site without any axial ligand [14]. Aging in ambient conditions therefore likely modified these sites into L-Fe(III)-N_4

sites, possibly as a result of carbon surface corrosion. The additional axial ligand (L) could be H_2O (from water vapor in ambient air) or axial ligand produced during carbon corrosion (in particular, nitrogen containing fragments as byproducts of N-C corrosion could axially bind a Fe-N_4 site).

3.4 Discussion

Combining the results of chemical, physical and electrochemical techniques, we now seek at highlighting the similarities but also the differences of ageing between the catalysts. We first emphasize that the deactivation phenomenon reported in this study is not specific to a given type of Fe-N-C catalyst but seems to be universal for this class of materials. For the UCI-2 and IQSC materials, a slight decrease in SD and a strong decrease in the TOF were noticed (**Figure 3**). In contrast, the CNRS-RP catalyst experienced a pronounced decrease in SD but almost no change in TOF. Local X-EDS analyses confirmed these trends, and elemental mappings as well as HERFD-XANES and XES analyses indicated that the oxidation state of Fe atoms increased in the aged CNRS-RP catalyst. The UCI-1 material is an exception, with an apparent increase in SD (likely associated with surface carbon corrosion and the formation of FeO_x on the surface from Fe atoms initially present as bulk FeN_x sites) and a marked decrease of the TOF.

As no electrochemical potential (no electrolyte) was applied during storage under atmospheric conditions, and as all tested Fe-N-C materials were stored in closed flasks, we hypothesized that oxygen or water molecules contained in the air played a major role on the reported chemical and physical changes, and the associated irreversible loss in ORR performance. Indeed, atmospheric conditions place the Fe-N-C catalysts in a corrosion situation, where oxygen act as an oxidant (towards the carbon matrix and the single Fe atoms) and the small amount of water adsorbed on

surface act as electrolyte (although of limited ionic conductivity). To verify our hypothesis, we compare in **Figure 7** the X-ray photoelectron spectra measured on the pristine and 24-month aged UCI-2 and CNRS-FP catalysts.

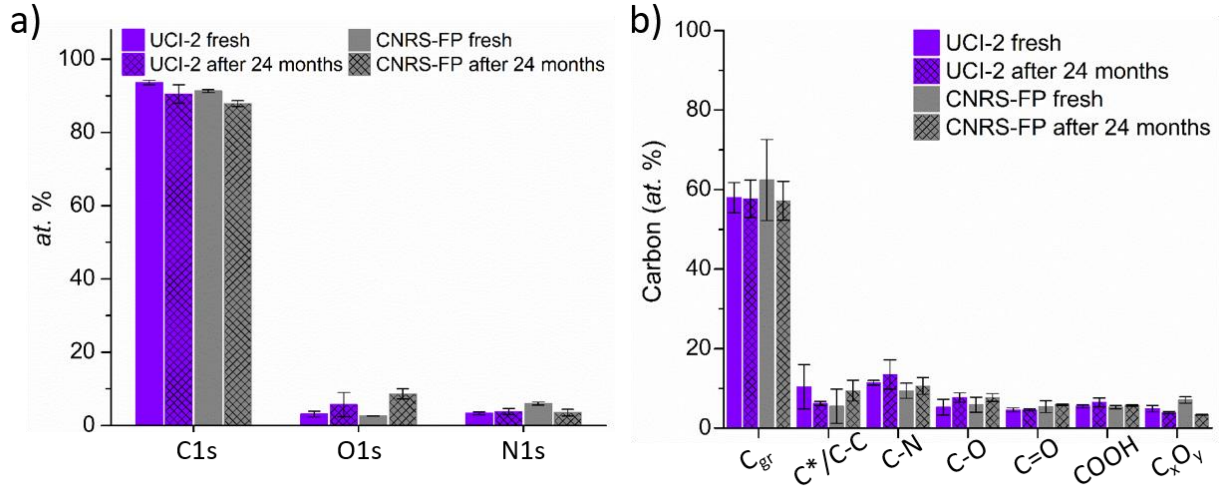

Figure 7. a) Variation of the content in oxygen, carbon and nitrogen monitored from O1s, C1s and N1s bands in X-ray photoelectron spectra and b) concentration of the functional groups present on carbon as derived from the deconvolution of the C1s band.

The O1s/C1s atomic ratio measured by XPS increased from 3.3 % to 6.3 % during storage under atmospheric conditions for the UCI-2 catalyst. The increase in oxygen content was even more impressive for the CNRS-FP catalyst: the O1s/C1s ratio changed from 2.8 % to 9.8 % during storage for 24 months under atmospheric conditions. Deconvolution of the C1s narrow scan spectrum into different functional groups indicates that the increase in oxygen content mostly arose from the formation of C-O groups (the raw C1s and N1s spectra for CNRS-FP and UCI-2 are provided in Supporting Information, see **Figure S4**). Corrosion of the surface and outermost layers of the carbon matrix then facilitates the aggregation (likely as Fe oxide) of single Fe atoms initially coordinated by nitrogen, as revealed from HAADF-STEM images (**Figure 4**). In

agreement with this scenario, the combined XANES and XES spectra of **Figure 6** show that the oxidation state of single Fe atoms increased, and that it was accompanied by change in their local coordination sphere, as expected from additional coordination with water molecules or COR products. Keeping this idea in mind, the less pronounced decrease in the SD reported for double-pyrolysed UCI-2 catalyst (in comparison to single-pyrolysed UCI-1 catalyst) can be explained by considering that the weakly-ordered carbon phase present in the Fe-N-C after a single pyrolysis was selectively removed during the NH_3 treatment (preferential reaction between NH_3 and the disordered carbon phase), and the carbon support left after the NH_3 pyrolysis corroded less during storage under atmospheric conditions.

To further confirm the key role of oxygen and/or water contained in air, the CNRS-FP was stored for 24 months in an Ar-purged glovebox, while the ARMINES catalyst was stored for 24 months in a desiccator. No loss in ORR activity was observed for the CNRS-FP catalyst (**Figure S5**), confirming that O_2 is required to promote the deactivation phenomenon reported here, which we named *spontaneous aerobic ageing*. This experiment also indicated that storage under Ar glovebox is an efficient way to mitigate the adverse effects of this phenomenon. In contrast, we noticed that the loss in ORR mass activity of the ARMINES catalyst was *ca* 25 % lower when stored in an Ar glovebox in comparison to storage for the same period of time in the desiccator (**Figure S5**). This result makes sense as desiccator protects samples from moisture not from oxygen. We also stress that the decrease in MA upon storage under atmospheric conditions was irreversible and independent on the metal. Indeed, the ORR activity could not be restored, even partially, using the electrochemical reduction protocol of Boldrin *et al.* [30] for 24-month or 47-month aged Fe-N-C catalysts (aged UCI-1 and aged ARMINES, 30, 60 or 300 s of reductive polarization at -0.3 V *vs*. RHE in 0.1 M H_2SO_4, see **Figure S6**). In contrast, the 53-month aged

UCI-1 material could be fully reactivated using the pyrolysis conditions (600°C, Ar atmosphere, 1h) proposed by Boldrin *et al*. (**Figure S7**). The differences between reductive polarization and thermal treatment are not surprising in view of the different energy supplied to the aged material to restructure during these reactivation processes. Let us also point that, even if the initial mass activity could be recovered and even slightly exceeded with the thermal reactivation process, the atomic-scale structure of the active sites is likely to be different in the pristine and thermally-reactivated UCI-1 catalysts. Different SD and TOF values measured on the pristine and thermally-treated UCI-1 catalyst support this hypothesis: the results provided in **Table S3** indicate that a small number of active sites with high TOF controls the ORR activity for the pristine UCI-1. In contrast, the ORR activity of the thermally-reactivated UCI-1 catalyst is controlled by the density of (poorly-active) catalytic surface sites. Thermal reactivation of the UCI-1 catalyst, however, is an important result that confirms the outcomes presented in the seminal study by Boldrin *et al*. [30]. Discussing no reactivation of the aged UCI-1 and ARMINES catalysts during reductive polarization, we would like to stress the important difference between the study of Boldrin *et al*. [30] and this study regarding the time scale:

- Either only 24 h cumulative exposure to O_2 (and in fact only 1 h continuous exposure, repeated 24 times) or one year storage under atmospheric conditions in Boldrin *et al.* [30],

- The present study: up to 47 months exposure to atmospheric conditions

The complete reactivation of the Imperial College London material [30] after one-year ambient air storage therefore suggests that oxygen-containing groups formed during one year of storage under atmospheric conditions were “reversible” *i.e.* they can be electrochemically reduced or

desorbed and the ORR activity could be restored. Conversely, the loss of ORR activity assessed in our study was "irreversible", at least for the UCI-1 and ARMINES catalysts, suggesting that the corrosion of the carbon matrix during four years led to irreversible changes in structure, chemistry and electrocatalytic activity. We can only point at the longer duration of air exposure in the present study, or different susceptibility of Fe-N-C catalysts to surface COR, to explain the difference between the present study and the study of Boldrin *et al*. [30].

Finally, in an effort to generalize our findings to different types of Metal-N-C catalysts but also to benchmark carbon-supported Pt nanoparticles used in the field of PEMFC, the ageing in ambient condition was studied on a Co-N-C material synthesized using the same synthesis protocol as CNRS-RP (Co-CNRS-RP), and first introduced in Ref. [21], and on a benchmark Pt/Vulcan XC72 catalyst (TEC10V20E from Tanaka Kikinzoku Kogyo, TKK). We found that nearly 60 % of the ORR mass activity measured at E = 0.8V *vs.* RHE was lost after 58 months of storage under atmospheric conditions for the Co-CNRS-RP catalyst (see **Figure S8)**. In contrast, no loss of ORR activity was observed for the benchmark Pt/Vulcan XC72 catalyst stored for more than 6 years in the same conditions (see **Figure S9**). However, the nature of the active sites in Pt/C and Fe-N-C catalysts is intrinsically different: Fe-N-C rely on single Fe cations embedded into a N-doped carbon matrix with specific surface area exceeding 500-600 m^2 g^{-1} hence any change in structure or chemistry of these active sites affects their SD and TOF values. In contrast, active sites are located onto the surface of Pt nanoparticles (*ca*. 3 nm in size *i.e*., containing several thousands of atoms) and Vulcan XC72 is a carbon black produced by partial oxidation of hydrocarbons, with specific surface area *ca*. 250 m^2 g^{-1}. Movements of Pt nanoparticles onto the Vulcan XC72 support, such as those caused by surface COR, are thus

unlikely to irreversibly damage the active sites of Pt/C nanoparticles, and it was no surprise to note that the ORR specific activity did not change over time.

CONCLUSIONS

We report here that Fe-N-C materials comprising single iron atom sites, the most broadly used non-platinum-group metal catalysts for the oxygen reduction reaction in acidic electrolyte, loose mass activity when stored under atmospheric conditions for long period of time. Six Fe-N-C materials prepared by different methods were studied. Electron microscopy identified spontaneous aggregation of single Fe atoms into Fe or Fe-oxide aggregates for some catalysts. The magnitude of the ORR activity loss however depends much on the preparation method of the Fe-N-C material. Even more complex, the deconvolution of the ORR mass activity into the site density, measured by *in situ* nitrite stripping method, and the turnover frequency reveals that some Fe-N-C materials show a strong decrease in turnover frequency but a mild decrease in site density, while other Fe-N-C materials show the opposite behavior. The catalytic de-activation after 4 years could not be restored by reductive electrochemical treatment, but could be restored by a thermal treatment under argon at 600°C. A similar aging phenomenon was also observed on a single-metal-atom Co-N-C catalyst synthesized using the same synthesis protocol as CNRS-RP catalyst, except for the nature of the transition metal. In contrast, no loss of the mass or specific activity towards the oxygen reduction reaction was observed for a benchmark Pt/C catalyst. Oxygen and water proved responsible for the deactivation process, and storage under dry argon helped mitigating the adverse effects of spontaneous aerobic ageing, while packaging under vacuum would very likely yield similar result.

CRediT authorship contribution statement

Keyla Teixeira Santos: Sample collection and analysis; Investigation; Formal analysis; Drawing; Data curation; Writing - original draft. **Kavita Kumar**: Sample collection and analysis; Investigation; Formal analysis; Drawing; Data curation. **Laetitia Dubau**: STEM/X-EDS measurements; Formal analysis; Data curation. **Hongxin Ge**: Materials synthesis and characterization, Investigation, Formal analysis, Data curation. **Sandrine Berthon-Fabry**: Project administration, Formal analysis, Data curation. **Carlos Vasconcelos**: Materials synthesis and characterization, Investigation, Formal analysis, Data curation. **Fabio Lima**: Materials synthesis, Project administration, Data curation. **Tristan Asset:** Material synthesis and characterization, X-ray Photoelectron Spectroscopy formal analysis; Data curation. **Plamen Atanassov**: Project administration. **Viktoriia A. Saveleva**: X-ray absorption spectroscopy and X-ray emission spectroscopy measurements; Formal analysis; Data curation. **Pieter Glatzel**: X-ray absorption spectroscopy and X-ray emission spectroscopy measurements; Formal analysis; Data curation. **Xiaoyan Li**: HR-TEM measurements, Formal analysis, Data curation. **Frédéric Jaouen**: Funding acquisition; Project administration; Resources; Validation, Writing – review & editing. **Frédéric Maillard**: Conceptualization; Data curation; Drawing; Formal analysis; Funding acquisition; Methodology; Project administration; Resources; Supervision; Validation; Visualization; Writing – review & editing.

Declaration of Competing Interest

The authors declare that they have no known competing financial interests or personal relationships that could have appeared to influence the work reported in this paper.

Appendix A. Supporting information

Supplementary data associated with this article can be found in the online version at DOI.

Acknowledgements

Science is also about sharing passion, exchanging ideas and enjoying life: we dedicate this work to the 60th birthday of our friend and colleague, Prof. Plamen Atanassov. This work was performed within the framework of the Centre of Excellence of Multifunctional Architectured Materials "CEMAM" n◦ ANR-10-LABX-44-01. The authors thank the European Synchrotron Radiation facility for provision of synchrotron radiation facilities at beamline ID06, and gratefully acknowledge financial support from the French National Research Agency through the ANIMA (grant number ANR-19-CE05-0039) project. K.T.S. acknowledges Coordenação de Aperfeiçoamento de Pessoal de Nível Superior (CAPES) Brazil (grant number 88887.598551/2021-00) and CAPES/COFECUB program (grant numbers: 88887-187755/2018-00 and Ph-C 914/18). C.V. and F.H.B.L. are thankful to the São Paulo State Research Foundation (FAPESP – grant number: 2019/22183-6) and Conselho Nacional de Desenvolvimento Científico e Tecnológico (CNPq – grant number: #309465/2019-2). We thank Nicolas Bibent (ICGM) for performing the reactivation pyrolysis. Dr. K. Teixeira Santos and Dr. K. Kumar contributed equally to this work.

References

[1] X. Wan, X. Liu, Y. Li, R. Yu, L. Zheng, W. Yan, H. Wang, M. Xu, J. Shui, Fe–N–C electrocatalyst with dense active sites and efficient mass transport for high-performance proton exchange membrane fuel cells. Nat. Catal., 2 (2019) 259-268. https://doi.org/10.1038/s41929-019-0237-3.

[2] T. Asset, P. Atanassov, Iron-nitrogen-carbon catalysts for proton exchange membrane fuel cells. Joule, 4 (2020) 33-44. https://doi.org/10.1016/j.joule.2019.12.002.

[3] T. Asset, F. Maillard, F. Jaouen, Electrocatalysis with single-metal atom sites in doped carbon matrices, in: Supported metal single atom catalysis, 2022, pp. 531-582. https://doi.org/10.1002/9783527830169.ch13.

[4] A.A. Gewirth, J.A. Varnell, A.M. DiAscro, Nonprecious metal catalysts for oxygen reduction in heterogeneous aqueous systems. Chem. Rev., 118 (2018) 2313-2339. https://doi.org/10.1021/acs.chemrev.7b00335.

[5] H. Yang, L. Shang, Q. Zhang, R. Shi, G.I.N. Waterhouse, L. Gu, T. Zhang, A universal ligand mediated method for large scale synthesis of transition metal single atom catalysts. Nat. Commun., 10 (2019) 4585. https://doi.org/10.1038/s41467-019-12510-0.

[6] S. Pylypenko, S. Mukherjee, T.S. Olson, P. Atanassov, Non-platinum oxygen reduction electrocatalysts based on pyrolyzed transition metal macrocycles. Electrochim. Acta, 53 (2008) 7875-7883. https://doi.org/10.1016/j.electacta.2008.05.047.

[7] E. Proietti, F. Jaouen, M. Lefevre, N. Larouche, J. Tian, J. Herranz, J.P. Dodelet, Iron-based cathode catalyst with enhanced power density in polymer electrolyte membrane fuel cells. Nat. Commun., 2 (2011) 416. https://doi.org/10.1038/ncomms1427.

[8] S. Ma, G.A. Goenaga, A.V. Call, D.J. Liu, Cobalt imidazolate framework as precursor for oxygen reduction reaction electrocatalysts. Chem. - Eur. J., 17 (2011) 2063-2067. https://doi.org/10.1002/chem.201003080.

[9] V. Armel, J. Hannauer, F. Jaouen, Effect of ZIF-8 crystal size on the O_2 electro-reduction performance of pyrolyzed Fe–N–C catalysts. Catalysts, 5 (2015) 1333-1351. https://doi.org/10.3390/catal5031333.

[10] Z. Jiang, J. Yu, T. Huang, M. Sun, Recent advance on polyaniline or polypyrrole-derived electrocatalysts for oxygen reduction reaction. Polymers, 10 (2018) 1397. https://doi.org/10.3390/polym10121397.

[11] L. Jiao, J. Li, L.L.R. Richard, Q. Sun, T. Stracensky, E. Liu, M.T. Sougrati, Z. Zhao, F. Yang, S. Zhong, H. Xu, S. Mukerjee, Y. Huang, D.A. Cullen, J.H. Park, M. Ferrandon, D.J. Myers, F. Jaouen, Q. Jia, Chemical vapour deposition of Fe–N–C oxygen reduction catalysts with full utilization of dense Fe–N_4 sites. Nature Mater., 20 (2021) 1385-1391. https://doi.org/10.1038/s41563-021-01030-2.

[12] A. Mehmood, M. Gong, F. Jaouen, A. Roy, A. Zitolo, A. Khan, M.-T. Sougrati, M. Primbs, A.M. Bonastre, D. Fongalland, G. Drazic, P. Strasser, A. Kucernak, High loading of single atomic iron sites in Fe–NC oxygen reduction catalysts for proton exchange membrane fuel cells. Nat. Catal., 5 (2022) 311-323. https://doi.org/10.1038/s41929-022-00772-9.

[13] J. Barrio, A. Pedersen, S. Ch. Sarma, A. Bagger, M. Gong, S. Favero, C.-X. Zhao, R. Garcia-Serres, A.Y. Li, Q. Zhang, F. Jaouen, F. Maillard, A. Kucernak, I.E.L. Stephens, M.-M.

Titirici, FeNC oxygen reduction electrocatalyst with high utilisation penta-coordinated sites. Adv. Mater., n/a (2023) 2211022. https://doi.org/10.1002/adma.202211022.

[14] K. Kumar, L. Dubau, M. Mermoux, J. Li, A. Zitolo, J. Nelayah, F. Jaouen, F. Maillard, On the Influence of Oxygen on the Degradation of Fe-N-C Catalysts. Angew. Chem. Int. Ed., 59 (2020) 3235-3243. https://doi.org/https://doi.org/10.1002/anie.201912451.

[15] L. Osmieri, D.A. Cullen, H.T. Chung, R.K. Ahluwalia, K.C. Neyerlin, Durability evaluation of a Fe–N–C catalyst in polymer electrolyte fuel cell environment via accelerated stress tests. Nano Energy, 78 (2020) 105209. https://doi.org/10.1016/j.nanoen.2020.105209.

[16] R. Chenitz, U.I. Kramm, M. Lefèvre, V. Glibin, G. Zhang, S. Sun, J.-P. Dodelet, A specific demetalation of Fe–N4 catalytic sites in the micropores of NC_Ar + NH_3 is at the origin of the initial activity loss of the highly active Fe/N/C catalyst used for the reduction of oxygen in PEM fuel cells. Energy Environ. Sci., 11 (2018) 365-382. https://doi.org/10.1039/c7ee02302b.

[17] X. Yin, P. Zelenay, Kinetic models for the degradation mechanisms of PGM-free ORR catalysts ECS Trans., 85 (2018) 1239-1250. https://doi.org/10.1149/08513.1239ecst.

[18] C.H. Choi, C. Baldizzone, J.P. Grote, A.K. Schuppert, F. Jaouen, K.J. Mayrhofer, Stability of Fe-N-C catalysts in acidic medium studied by *operando* spectroscopy. Angew. Chem. Int. Ed., 54 (2015) 12753-12757. https://doi.org/10.1002/anie.201504903.

[19] C.H. Choi, C. Baldizzone, G. Polymeros, E. Pizzutilo, O. Kasian, A.K. Schuppert, N. Ranjbar Sahraie, M.-T. Sougrati, K.J.J. Mayrhofer, F. Jaouen, Minimizing *operando* demetallation of Fe-N-C electrocatalysts in acidic medium. ACS Catal., 6 (2016) 3136-3146. https://doi.org/10.1021/acscatal.6b00643.

[20] C.H. Choi, H.-K. Lim, M.W. Chung, G. Chon, N. Ranjbar Sahraie, A. Altin, M.-T. Sougrati, L. Stievano, H.S. Oh, E.S. Park, F. Luo, P. Strasser, G. Dražić, K.J.J. Mayrhofer, H. Kim, F.

Jaouen, The Achilles' heel of iron-based catalysts during oxygen reduction in an acidic medium. Energy Environ. Sci., 11 (2018) 3176-3182. https://doi.org/10.1039/c8ee01855c.

[21] K. Kumar, P. Gairola, M. Lions, N. Ranjbar-Sahraie, M. Mermoux, L. Dubau, A. Zitolo, F. Jaouen, F. Maillard, Physical and chemical considerations for improving catalytic activity and stability of non-precious-metal oxygen reduction reaction catalysts. ACS Catal., 8 (2018) 11264-11276. https://doi.org/10.1021/acscatal.8b02934

[22] K. Kumar, T. Asset, X. Li, Y. Liu, X. Yan, Y. Chen, M. Mermoux, X. Pan, P. Atanassov, F. Maillard, L. Dubau, Fe–N–C electrocatalysts' durability: Effects of single atoms' mobility and clustering. ACS Catal., 11 (2021) 484-494. https://doi.org/10.1021/acscatal.0c04625.

[23] J. Li, M.T. Sougrati, A. Zitolo, J.M. Ablett, I.C. Oğuz, T. Mineva, I. Matanovic, P. Atanassov, Y. Huang, I. Zenyuk, A. Di Cicco, K. Kumar, L. Dubau, F. Maillard, G. Dražić, F. Jaouen, Identification of durable and non-durable FeN_x sites in Fe–N–C materials for proton exchange membrane fuel cells. Nat. Catal., 4 (2021) 10-19. https://doi.org/10.1038/s41929-020-00545-2.

[24] Q. Jia, N. Ramaswamy, U. Tylus, K. Strickland, J. Li, A. Serov, K. Artyushkova, P. Atanassov, J. Anibal, C. Gumeci, S.C. Barton, M.T. Sougrati, F. Jaouen, B. Halevi, S. Mukerjee, Spectroscopic insights into the nature of active sites in iron–nitrogen–carbon electrocatalysts for oxygen reduction in acid. Nano Energy, 29 (2016) 65-82. https://doi.org/10.1016/j.nanoen.2016.03.025.

[25] P.G. Santori, F.D. Speck, J. Li, A. Zitolo, Q. Jia, S. Mukerjee, S. Cherevko, F. Jaouen, Effect of pyrolysis atmosphere and electrolyte pH on the oxygen reduction activity, stability and spectroscopic signature of FeN_x moieties in Fe-N-C catalysts. J. Electrochem. Soc., 166 (2019) F3311-F3320. https://doi.org/10.1149/2.0371907jes.

[26] E.F. Holby, G. Wang, P. Zelenay, Acid stability and demetalation of PGM-free ORR electrocatalyst structures from density functional theory: A model for "single-atom catalyst" dissolution. ACS Catal., 10 (2020) 14527-14539. https://doi.org/10.1021/acscatal.0c02856.

[27] L. Castanheira, L. Dubau, M. Mermoux, G. Berthomé, N. Caqué, E. Rossinot, M. Chatenet, F. Maillard, Carbon corrosion in proton-exchange membrane fuel cells: From model experiments to real-life operation in membrane electrode assemblies. ACS Catal., 4 (2014) 2258-2267.

[28] L. Castanheira, W.O. Silva, F.H.B. Lima, A. Crisci, L. Dubau, F. Maillard, Carbon corrosion in proton-exchange membrane fuel cells: Effect of the carbon structure, the degradation protocol, and the gas atmosphere. ACS Catal., 5 (2015) 2184-2194. https://doi.org/10.1021/cs501973j.

[29] J. Herranz, F. Jaouen, M. Lefevre, U.I. Kramm, E. Proietti, J.P. Dodelet, P. Bogdanoff, S. Fiechter, I. Abs-Wurmbach, P. Bertrand, T.M. Arruda, S. Mukerjee, Unveiling N-protonation and anion-binding effects on Fe/N/C-catalysts for O_2 reduction in PEM fuel cells. J. Phys. Chem. C, 115 (2011) 16087-16097. https://doi.org/10.1021/jp2042526.

[30] P. Boldrin, D. Malko, A. Mehmood, U.I. Kramm, S. Wagner, S. Paul, N. Weidler, A. Kucernak, Deactivation, reactivation and super-activation of Fe-N/C oxygen reduction electrocatalysts: Gas sorption, physical and electrochemical investigation using NO and O_2. Appl. Catal., B, 292 (2021) 120169. https://doi.org/10.1016/j.apcatb.2021.120169

[31] Y. Wang, M.J. Larsen, S. Rojas, M.-T. Sougrati, F. Jaouen, P. Ferrer, D. Gianolio, S. Berthon-Fabry, Influence of the synthesis parameters on the proton exchange membrane fuel cells performance of Fe–N–C aerogel catalysts. J. Power Sources, 514 (2021) 230561. https://doi.org/10.1016/j.jpowsour.2021.230561.

[32] K. Artyushkova, I. Matanovic, B. Halevi, P. Atanassov, Oxygen binding to active sites of Fe–N–C ORR electrocatalysts observed by ambient-pressure XPS. J. Phys. Chem. C, 121 (2017) 2836-2843. https://doi.org/10.1021/acs.jpcc.6b11721.

[33] D. Malko, A. Kucernak, T. Lopes, *In situ* electrochemical quantification of active sites in Fe-N/C non-precious metal catalysts. Nat. Commun., 7 (2016) 13285. https://doi.org/10.1038/ncomms13285.

[34] H. Ge, N. Bibent, K. Teixeira Santos, K. Kumar, J. Jaxel, M. Sougrati, A. Zitolo, M. Dupont, F. Lecoeur, M. Mermoux, V. Martin, L. Dubau, F. Jaouen, F. Maillard, S. Berthon-Fabry, Fe-N-Carbon aerogel catalysts with high content of Fe-N_4 active sites for high performance oxygen reduction reaction. ACS Catal., 13 (2023) 1149-1163. https://doi.org/10.1021/acscatal.2c05394.

[35] U.I. Koslowski, I. Herrmann, P. Bogdanoff, C. Barkschat, S. Fiechter, N. Iwata, H. Takahashi, H. Nishikori, in: ECS Trans., 2008, pp. 125-141. https://doi.org/:10.1149/1.3039771.

[36] P. Glatzel, T.C. Weng, K. Kvashnina, J. Swarbrick, M. Sikora, E. Gallo, N. Smolentsev, R.A. Mori, Reflections on hard X-ray photon-in/photon-out spectroscopy for electronic structure studies. J. Electron Spectrosc. Relat. Phenom., 188 (2013) 17-25. https://doi.org/10.1016/j.elspec.2012.09.004.

[37] T.E. Westre, P. Kennepohl, J.G. DeWitt, B. Hedman, K.O. Hodgson, E.I. Solomon, A multiplet analysis of Fe K-edge 1s → 3d pre-edge features of iron complexes. J. Am. Chem. Soc., 119 (1997) 6297-6314. https://doi.org/10.1021/ja964352a.